Published in final edited form as:

Nanoscale. 2018 December 07; 10(45): 21369–21373. doi:10.1039/c8nr06262e.

Chelation-assisted assembly of multidentate colloidal nanoparticles into metal-organic nanoparticles

Yuan Liu[a,b], **Hao Sun**[c], **Lu Yang**[a], **Xiaochen Zhu**[d], **Xirui Wang**[e], **Jiamin Liang**[e], **Xiaowei Li**[a], **Ying Jiang**[a], **Weijia Hou**[a], **Caue Favero Ferreira**[e], **Daniel R. Talham**[e], **Arthur F. Hebard**[d], and **Weihong Tan**[a,b]

[a]Department of Chemistry and Physiology and Functional Genomics, Center for Research at the Bio/Nano Interface, Health Cancer Center, University of Florida, Gainesville, FL 32611-7200, USA, tan@chem.ufl.edu

[b]Molecular Science and Biomedicine Laboratory, State Key Laboratory of Chemo/Bio-Sensing and Chemometrics, College of Biology and College of Chemistry and Chemical Engineering, Hunan University, Changsha, 410082, China

[c]George & Josephine Butler Polymer Research Laboratory, Center for Macromolecular Science & Engineering, Department of Chemistry, University of Florida, Gainesville, Florida 32611-7200, USA

[d]Department of Physics, University of Florida, Gainesville, FL, 32611, USA

[e]Department of Chemistry, University of Florida, Gainesville, Florida

Abstract

We propose a chelation-assisted assembly of multidentate CNs into metal-organic nanoparticles (MONs). Multidentate CNs functionalized with coordination sites participate equally as organic linkers in MON construction, which is driven by chelation between metal ions and coordination sites. MONs assembled from Au nanoparticles display particle number- and size-dependent optical properties. In addition, the resulting CN-assembled MONs give evidence that assembly was dictated by the multidentate surface ligand rather than the size, shape or material of CNs. With this chelation-assisted strategy, it is possible to control the number of assembled CNs and build the connections between them.

Colloidal nanoparticles (CNs), also called ‘artificial atoms’, display unique physical and chemical properties owing to the nanoscale size effect, as well as significant collective properties upon assembly.[1–2] Assembly of CNs has been demonstrated to be a powerful tool to control the structure and properties of assembled nanoparticles for potential applications in, for example, catalysis, electrical devices, and biochemical sensors.[3–4] New optical, electronic, and magnetic properties can be obtained as a result of interactions between

Conflicts of interest

There are no conflicts to declare.

Electronic Supplementary Information (ESI) available: [details of any supplementary information available should be included here]. See DOI: 10.1039/x0xx00000x

closely packed individual nanoparticles.[2,5] Assembly of CNs can be governed by striking a balance among various forces such as van der Waals forces, hydrogen bonding and dipole interactions.[2,6] The assembly process can also be assisted by use of a template to generate electrical or magnetic fields.[7–8] Various structures, including 1D chains,[9–11] 2D sheets,[12] 3D crystals,[13–15] and 3D superparticles have been produced.[16] Several approaches including polymerization,[10,17] DNA templates,[3,18] or oil-in-water microemulsions[19–20] have been developed to trigger the assembly of CNs. However, despite recent successes, precise control over the assembly of CNs remains a challenge.

Metal-organic nanoparticles (MONs), constructed of metal ions and organic linkers with multiple coordination sites, have been explored for various applications, including drug delivery, optoelectronics, and chemical sensing.[21–23] The structure of MONs strongly depends on the coordination geometry of the metal ions, as well as the conformation, and coordination sites of the organic linkers. An important research goal is to fabricate MONs with novel composition to obtain interesting properties for new applications.[24] Mirkin et al. reported a class of metal-metalloligand particles which further enabled preparation of fluorescent MONs capable of storing hydrogen.[22,24,25] Inspired by the chelation of metal ions and organic linkers, we herein propose that multidentate inorganic CNs with coordination sites can be assembled into MONs via chelation between metal ions and coordination sites on organic linkers and CNs.

Considering our extensive experience in the design and synthesis of nanoarchitectures, we proposed that the thermal annealing of Zn^{2+} ions and Mn(III) meso-tetra (4-carboxyphenyl) porphine chloride (Mn-TCPP), which has four carboxylic acid coordination sites, would generate Zn-Mn-coordinated MONs (ZnMONs) in the presence of pyrazine and polyvinylpyrrolidone (PVP). Moreover, we reason that multidentate colloidal nanoparticles (Scheme 1) of different elements and functionalized with coordination sites could be incorporated into ZnMONs. To form the initial ZnMONs, a solution of Mn-TCPP in DMF/ethanol mixed solvent was added to another solution of $Zn(NO_3)_2$, pyrazine and PVP, also in DMF/ethanol. The resulting solution was then incubated in an oil bath at 80 °C for 24 hours. ZnMONs assembled with CNs were synthesized in a similar way, but multidentate CNs with carboxylate ligands (or capped with carboxylic acid-containing ligands after ligand exchange)[26] were introduced into the initial ZnMON mother solution and then incubated in an oil bath at 80 °C for 24 hours. The ZnMONs or CN-assembled ZnMONs were washed with ethanol and finally redispersed in ethanol.

The colloidal NPs and ZnMONs were characterized with transmission electron microscopy (TEM) (Fig. 1a, Fig. S1), powder X-ray diffraction (Fig. S2-S4) dynamic light scattering (DLS) (Fig. S5-S7), UV/Vis (Fig. S8), IR spectroscopy (Fig. S9) and X-ray photoelectron spectroscopy (XPS) (Fig. 1g and Fig. S10). Fig. 1a shows that ZnMONs are spherical with an average diameter of 120 ± 14 nm, while DLS measurement exhibited an average hydrodynamic diameter of 140 nm. According to UV/Vis spectra, an obvious change was observed in the Soret band (380–500 nm) of ZnMONs compared to Mn-TCPP. In addition, a red shift of Q band (500–750 nm) was observed and may be attributed to the assembly of Mn-TCPP upon chelation with zinc ions.[27] Infrared (IR) spectrum of Zn-MONs displayed characteristic peaks of alkane (C-H at 2930 cm^{-1}) and amide (C=O at 1660 cm^{-1}) from

PVP, as well as aromatic C=C (1605 cm^{-1}) signals from Mn-TCPP (Fig. S9). As a consequence of the overlap of the peaks for pyrazine and Mn-TCPP at 1630 cm^{-1} and 1400 cm^{-1}, it was not possible to determine from the IR spectra whether pyrazine participated in the construction of ZnMONs. Therefore, a control experiment involving ZnMON synthesis was carried out in the absence of pyrazine. However, no uniform ZnMONs were formed without pyrazine.

To incorporate multidentate CNs into the ZnMONs, we first synthesized aqueous Au nanoparticles (15 ± 1 nm) containing citrate as capping ligands. Aqueous Au nanoparticles (Au15) were concentrated by centrifugation and then redispersed in DMF. The concentrated Au nanoparticles were then added to the Zn^{2+}/PVP/pyrazine solution in DMF/ethanol prior to introducing Mn-TCPP. After incubation in an oil bath for 24 hours, uniform Au15-ZnMON core-shell structures were observed, as shown in the TEM images (Fig. 1b). We further studied the effect of Au-CN size on the assembly. Aqueous Au nanoparticles with different sizes and shapes (i.e., 25 nm spheres (Au25), 50 nm spheres (Au50) and nanorods 10 × 41 nm (AuNR)), but with the same citrate capping ligands, were used in the synthesis. TEM images demonstrate that all Au nanoparticles gave rise to uniform core-shell structures (Au15-ZnMON (Fig. 1b), Au25-ZnMON (Fig. 1c), Au50-ZnMON (Fig. 1d), and AuNR-MON (Fig. 1e)). Diameter and shell thickness are listed in Table 1. In addition, the size and shape of AuCNs did not affect the assembly of CNs. However, CN- assembled ZnMON was not observed when Au nanorods with same size and shape, but cetyltrimethylammonium bromide (CTAB) as capping ligand, were introduced to the ZnMON mother solution (Fig. 1f). This is because CTAB is incapable of chelating with Zn^{2+} as carboxylate, although CTAB-capped Au nanorods are aqueous and can be redispersed in DMF.

UV-vis absorption spectra of the Au nanoparticles, ZnMONs and AuNC-ZnMONs are shown in Fig. 2. No obvious difference was observed between ZnMONs and Au15-ZnMONs (Fig. 2a) indicating that the shell is also amorphous and assembled from metal ions and organic linkers with multi-coordination sites through coordination between Zn ions and carboxylic acid groups. As the sizes of Au nanoparticles increased, the surface plasmon peak at about 525 nm contributed more to the AuNC-ZnMON spectrum, resulting in a slight red shift (Fig.s 2b, 2c). For AuNRs (Fig. 2d), the surface plasmon band appears at about 800 nm, and the red shift in AuNR-ZnMONs is only 8 nm. These two red shifts are attributed to the intrinsic size effect of Au nanoparticles and an increase in the local refractive index around the Au nanoparticles.[28–30] However, the Soret band and the Q band of ZnMONs did not move at all after being assembled with Au nanoparticles, indicating that the incorporation of Au nanoparticles into ZnMONs did not affect the structure of ZnMONs. Fig. 3 shows the EDS line scan of Au15-ZnMONs, which confirms the chemical assignments and component segregation. Au nanoparticles as core show independent peaks (blue), whereas Mn (red) and Zn (green) are evenly distributed in ZnMONs.

Having demonstrated that citrate-modified multidentate Au nanoparticles can be assembled into ZnMONs by complexation with Zn^{2+} ions, we further extended the scope of the method with multidentate iron oxide and upconversion nanoparticles (UCNP), which were functionalized with 3,4-dihydroxyhydrocinnamic acid by ligand exchange. As shown in the TEM images, hexagonal UCNP and iron oxide can be incorporated into ZnMONs (Fig. 4b

and 4c). Original properties can arise from synergistic effects between the core and the shell of the particles. Singlet oxygen generation from the synergistic effect of UCNP/MON core shell structures was studied Due to spectra overlap of the emission of UCNP and absorption of Mn-TCPP from 510 nm to 560 nm, when UCNP was irradiated with 980 nm light, the photosensitizer Mn-TCPP would be excited by the emission of UCNP and generate singlet oxygen which can be potentially used for further photodynamic therapy (PDT). Singlet oxygen generation was monitored by SOSG as shown in fig. S11. The successful assembly of UCNP and iron oxide nanoparticles into ZnMONs indicates that it is the surface capping ligand (carboxylate), rather than the material itself, that dictates assembly.

Since each multidentate nanoparticle has equal opportunity to be assembled into ZnMONs, we assumed that the number of multidentate colloidal nanoparticles assembled into ZnMONs would be concentration-dependent. To elucidate this hypothesis, different concentrations of Au and iron oxide nanoparticles were used for assembly. As expected, more colloidal nanoparticles were assembled into ZnMONs as the concentration of CNs increased. In the case of Au15-ZnMON-1, 70% of ZnMONs each hold one Au15 nanoparticle and 18% of ZnMONs each hold two Au15 nanoparticles, while ZnMONs with three or more Au nanoparticles account for 6%. However, when six-fold of Au15 nanoparticles were added, as in the case of Au15-ZnMON-2, the ratio of ZnMONs holding two Au15 nanoparticles increased to 26% and ZnMONs with three or more Au nanoparticles increased to 42% (Fig. 5a and Fig. S12). A broad peak appeared around 560 nm after red shift confirmed the assembly of ZnMONs with 3 and above Au-15 nanoparticles (Fig. 5b).[31] Unfortunately, assembly was not successful when an excess of multidentate CNs was added, because Mn-TCPP and Zn ions would be limiting reagents. Similarly, we also observed an increase in the number of nanoparticles assembled into ZnMONs with increased concentration of multidentate iron oxide nanoparticles, as shown in Fig. 5c and 5d (Iron oxide11-ZnMON-1), 5e and 5f (Iron oxide11-ZnMON-2), and 5g and 5h (Iron oxide11-ZnMON-3). Therefore, the number of colloidal nanoparticles assembled into ZnMONs is concentration-dependent. Additionally, magnetic property variation of iron oxide/MON with different concentration of assembled iron oxide nanoparticles is revealed by the magnetization measurement. As shown in Fig. S13, all three samples demonstrated the typical superparamagnetic behavior, since neither remanent magnetization nor coercivity was detected.

Conclusions

In conclusion, we have developed a new chelation-assisted procedure to incorporate multidentate CNs into ZnMONs. The concentration of multidentate CNs allows for control over the number of CNs in ZnMONs. This assembly methodology is applicable to a library of colloidal nanoparticles with photoelectrochemical properties, such as semiconductor quantum dots and metal nanoparticles, as long as their multidentate surfaces are well developed. The incorporating multidentate CNs into ZnMONs by complexation will also open up many new opportunities for practical applications in biochemical and electrical areas.

Supplementary Material

Refer to Web version on PubMed Central for supplementary material.

Acknowledgements

The The authors are grateful to Dr. Kathryn Williams for her critical comments during the preparation of this manuscript. This work is supported by grants awarded by the National Institutes of Health (GM079359 and CA133086) and the National science foundation under the Division of Materials Research, Grant number DMR-1305783. It is also supported by grants awarded by the National Key Scientific Program of China (2011CB911000 and 2013CB933701), the Foundation for Innovative Research Groups of NSFC (Grant 21221003 and NSFC 21327009).

Notes and references

1. Macfarlane RJ, Lee B, Jones MR, Harris N, Schatz GC, Mirkin CA, Science, 2011 334, 204–208. [PubMed: 21998382]
2. Nie Z, Petukhova A, Kumacheva E, Nat. Nanotech, 2010 5, 15–25.
3. (a) Sun Z, Sun B, Qiao M, Wei J, Yue Q, Wang C, Deng Y, Kaliaguine S, Zhao D, J. Am. Chem. Soc 2012, 134, 17653–17660. [PubMed: 23020275] (b) Jone MR, Seeman NC, Mirkin CA, Science, 2015, 347, 1260901. [PubMed: 25700524]
4. Chen O, Riedemann L, Etoc F, Herrmann H, Coppey M, Barch M, Farrar CT, Zhao J, Bruns OT, Wei H, Guo P, Cui J, Jensen R, Chen Y, Harris DK, Cordero JM, Wang Z, Jasanoff A, Fukumura D, Reimer R, Dahan M, Jain RK, Bawendi MG, Nat. Commun, 2014, 5, 5093–5100. [PubMed: 25298155]
5. Kuzyk A, Schreiber R, Fan Z, Pardatscher G, Roller E, Hogele A, Simmel FC, Govorov AO, Liedl T, Nature, 2012, 483, 311–314. [PubMed: 22422265]
6. Zeng C, Chen Y, Kirschbaum K, Lambright KJ, Jin R, Science, 2016, 354, 1580–1584. [PubMed: 28008066]
7. Bishop KJM, Wilmer CE, Soh S, Grzybowski BA, Small, 2009, 5, 1600–1630. [PubMed: 19517482]
8. Lalatonne Y, Richardi J, Pileni MP, Nat. Mater, 2004, 3, 121–125. [PubMed: 14730356]
9. Shen X, Chen L, Li D, Zhu L, Wang H, Liu C, Wang Y, Xiong Q, Chen H, ACS Nano, 2011, 5, 8426–8433. [PubMed: 21942743]
10. Nie Z, Fava D, Kumacheva E, Zou S, Walker GC, Rubinstein M, Nat. Mater, 2007, 6, 609–614. [PubMed: 17618291]
11. Kim PY, Oh J, Nam J, J. Am. Chem. Soc, 2015, 137, 8030–8033. [PubMed: 26067225]
12. Tang Z, Zhang Z, Wang Y, Glotzer SC, Kotov NA, Science, 2006, 314, 274–278. [PubMed: 17038616]
13. Zhang J, Santos PJ, Gabrys PA, Lee S, Liu C, Macfarlane RJ, J. Am. Chem. Soc, 2016, 138, 16228–16231. [PubMed: 27935680]
14. Henzie J, Grünwald M, Widmer-Cooper A, Geissler PL, Yang P, Nat. Mater, 2011, 11, 131–137. [PubMed: 22101811]
15. Talapin DV, Shevchenko EV, Bodnarchuk MI, Ye X, Chen J, Murray CB, Nature, 2009, 461, 964–967. [PubMed: 19829378]
16. Wang T, Zhuang J, Lynch J, Chen O, Wang Z, Wang X, LaMontagne D, Wu H, Wang Z, Cao YC, Science, 2012, 338, 358–363. [PubMed: 23087242]
17. Liu K, Nie Z, Zhao N, Li W, Rubinstein M, Kumacheva E, Science, 2010, 329, 197–200. [PubMed: 20616274]
18. Roger WB, Shih WM, Manoharan VN, Nat. Rev. Mater, 2016, 1, 16008–16021.
19. Wang T, LaMontagne D, Lynch J, Zhuang J, Cao YC, Chem. Soc. Rev, 2013, 42, 2804–2823. [PubMed: 23104182]
20. Boles MA, Engel M, Talapin DV, Chem. Rev, 2016, 116, 11220–11289. [PubMed: 27552640]

21. Carné A, Carbonell C, Imaz I, Maspoch D, Chem. Soc. Rev, 2011, 40, 291–305. [PubMed: 21107481]
22. Oh M, Mirkin CA, Nature, 2005, 438, 651–654. [PubMed: 16319888]
23. Sun X, Dong S, Wang E, J. Am. Chem. Soc, 2005, 127, 13102–13103. [PubMed: 16173711]
24. Oh M, Mirkin CA, Angew. Chem. Int. Ed, 2006, 45, 5492–5494.
25. Jeon Y, Armatas GS, Heo J, Kanatzidis MG, Mirkin CA, Adv. Mater, 2008, 20, 2105–2110.
26. Liu Y, Purich DL, Wu C, Wu Y, Chen T, Cui C, Zhang L, Cansiz S, Hou W, Wang Y, Yang S, Tan W, J. Am. Chem. Soc, 2015, 137, 14952–14958. [PubMed: 26562739]
27. Zhao M, Wang Y, Ma Q, Huang Y, Zhang X, Ping J, Zhang Z, Lu Q, Yu Y, Xu H, Zhao Y, Zhang H, Adv. Mater, 2015, 27, 7372–7378. [PubMed: 26468970]
28. Ghosh SK, Pal T, Chem. Rev, 2007, 107, 4797–4862. [PubMed: 17999554]
29. Piliarik M, Kvasnička P, Galler N, Krenn JR, Homola J, Opt J. Express, 2011, 19, 9213–9220.
30. Kang H, Trondoli AC, Zhu G, Chen Y, Chang Y, Liu H, Huang Y, Zhang X, Tan W, ACS Nano, 2011, 5, 5094–5099. [PubMed: 21542633]
31. Urban AS, Shen X, Wang Y, Large N, Wang H, Knight MW, Nordlander P, Chen H, Halas NJ, Nano Lett, 2013, 13, 4399–4403. [PubMed: 23977943]
32. Grabar KC, Freeman RG, Hommer MB, Natan MJ, Anal. Chem, 1995, 67, 735–743.

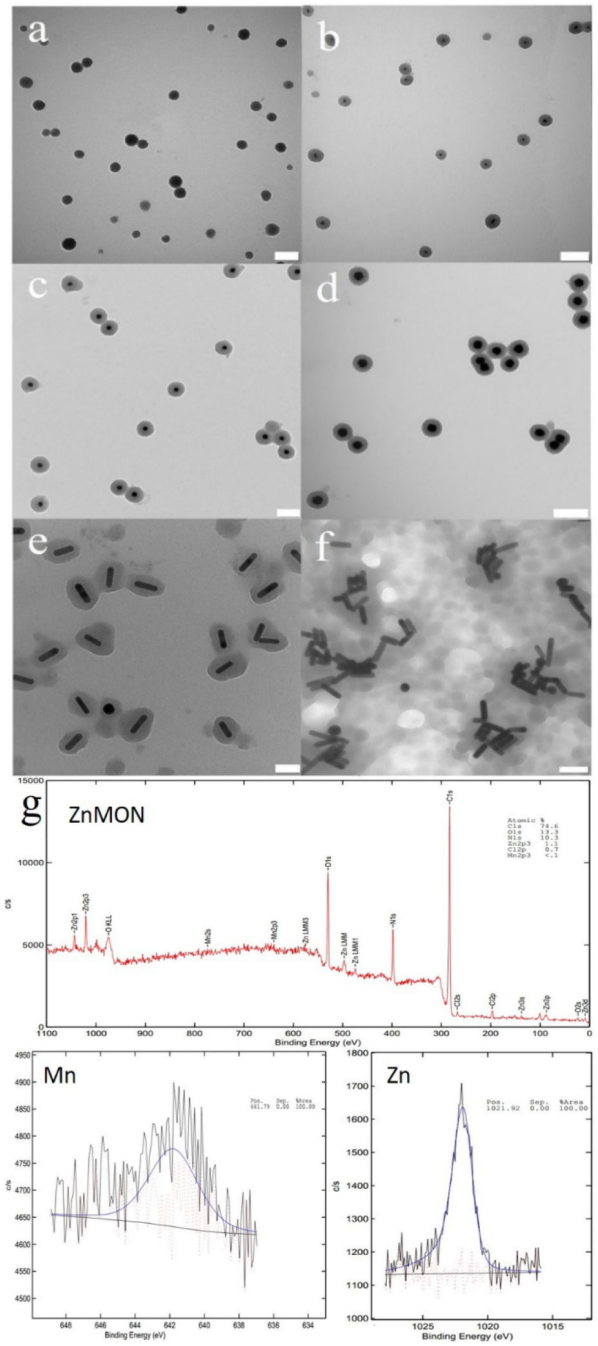

Fig. 1.

TEM images of (a) Zn-MONs, (b) Au15-ZnMON, (c) Au25-ZnMON, (d) Au50-ZnMON, (e) AuNR-ZnMON, and (f) CTAB-capped Au nanorods assembly. (g) XPS of ZnMOF. Scale bars: a, b, and d 200 nm; c 100 nm; e, f 50 nm.

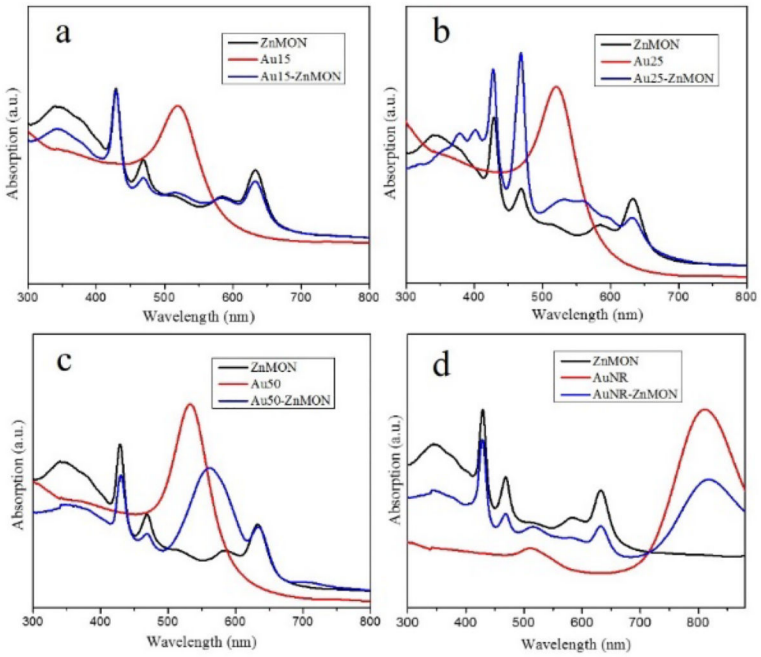

Fig. 2.

UV-vis spectra of ZnMON, Au nanoparticles and corresponding Au nanoparticles incorporated into ZnMONs. (a) Au15 and Au15-ZnMONs, (b) Au25 and Au25-ZnMONs, (c) Au50 and Au50-ZnMONs, (d) AuNR and AuNR-ZnMONs

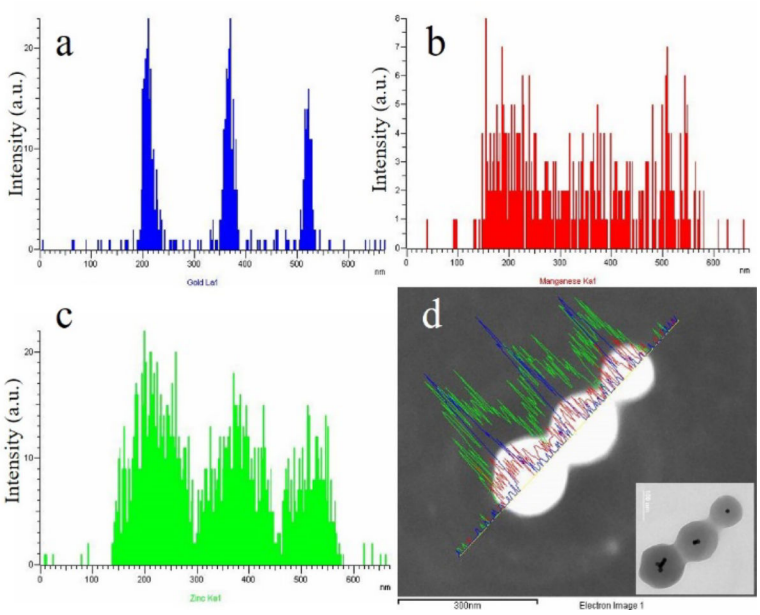

Fig. 3.

EDS line scans on Au15-ZnMONs. Data indicate the counts for each element detected as a function of the position of the electron beam across the particles. (a) is the signal of gold; (b) is the signal of Mn; (c) is the signal of Zn; (d) combined signals of the line scan. Inset: corresponding TEM image.

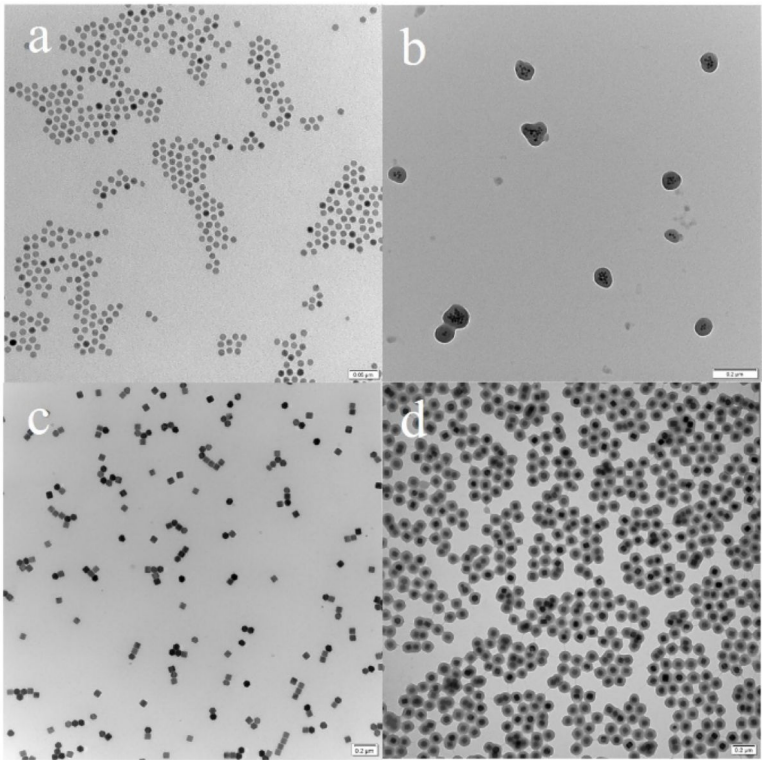

Fig. 4.

TEM images of iron oxide (11 nm) before assembly (a) and after incorporation into ZnMONs (b), UCNP before (c) and after incorporation into ZnMONs (d). Scale bar: a 50 nm; b, c, and d 200 nm.

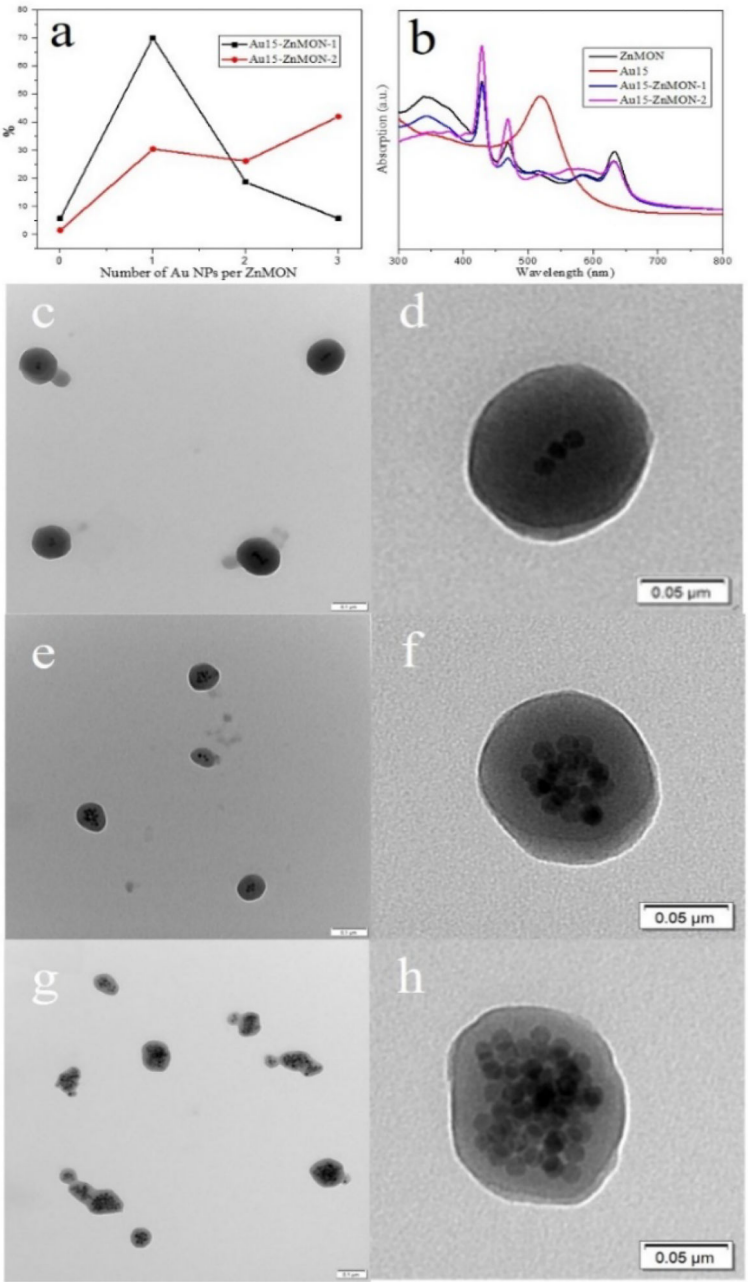

Fig. 5.

(a) Distribution of ZnMONs containing different numbers of Au15 nanoparticles (the number three means ZnMONs holding three or more Au15 nanoparticles); (b) Comparison of UV-vis absorption of Au15-ZnMON-1 and Au15-ZnMON-2. (c-h) TEM images of ZnMONs assembled with different numbers of multidentate iron oxide nanoparticles (d is the zoom of c; f is the zoom of e; and h is the zoom of g. Compared with Iron oxide11-ZnMON-1, 6 times the number of iron oxide nanoparticles were added to form Iron oxide11-ZnMON-2, and 12 times the number of iron oxide nanoparticles were added to form Iron oxide11-ZnMON-3). Scale bar: c, e, g 100 nm; d, f, h 50 nm.

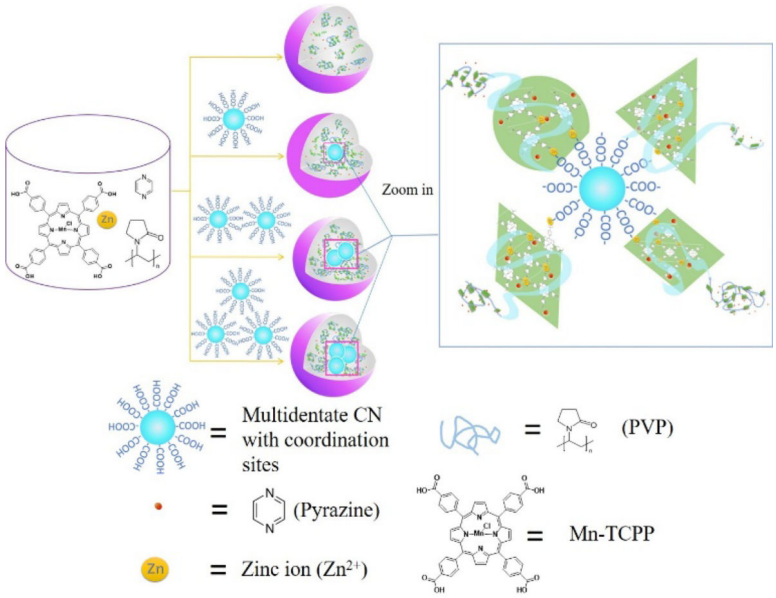

Scheme 1.
Synthesis of ZnMONs and the assembly of CNs into ZnMONs.

Table 1.

Size information of multidentate CNs assembled ZnMONs.

	Diameter (nm)	Shell thickness (nm)
Au15-ZnMON	105 ± 5	44 ± 3
Au25-ZnMON	103 ± 3	38 ± 2
Au50-ZnMON	124 ± 4	35 ± 2
AuNR-ZnMON	90 (±4) × 66 (±4)	22 ± 3